Scanning-electron-microscope technique for measuring electrical conductivity: Application to tetrathiafulvalene-tetracyanoquinodimethane

James P. Long* and Charles P. Slichter
Department of Physics and Materials Research Laboratory, University of Illinois, Urbana-Champaign, Illinois 61801
(Received 16 November 1979)

A new technique for measuring the electrical conductivity of small samples and its application to the organic conductor tetrathiafulvalene-tetracyanoquinodimethane (TTF-TCNQ) is reported. A movable current source provided by the electron beam of a scanning electron microscope is used to map out the potential distribution on crystal faces containing the a-b crystallographic axes. Silver paint contacts are used to return the beam current to ground and measure voltage changes as the beam position is moved. The results of the new technique are confirmed and complemented by the conventional movable-contact method and the extension of both methods to low temperature is discussed. The potential distributions for our samples reveal frequently occurring irregularities which are attributable to sample imperfections and inhomogeneities in the silver paint contacts. Methods are presented whereby the conductivities σ_a and σ_b can be determined despite the presence of certain current flow irregularities; room-temperature values are found to be $\sigma_b = 490 \pm 80\ (\Omega\,\mathrm{cm})^{-1}$ and $\sigma_a = 1.21 \pm 0.15\ (\Omega\,\mathrm{cm})^{-1}$. The relationship of σ_a and σ_b to the elements of the monoclinic conductivity tensor for TTF-TCNQ is clarified. The influence of contact inhomogeneities on four-probe measurements of the temperature dependence of $\sigma_b(T)$ as determined with an electrolytic tank model are presented as is an evaluation of two simple tests which detect measurements influenced by current-flow irregularities. In the tank, contact inhomogeneities are found responsible for erroneously large measurements of $\sigma_b(T)$ which occur with small probability and which resemble published data.

I. INTRODUCTION

The organic conductor tetrathiafulvalene-tetracyanoquinodimethane (TTF-TCNQ) exhibits an anisotropy in its room-temperature b-axis–a-axis electrical conductivity of about 400:1. The large anisotropy in this and other molecular crystals[1,2] has motivated extensive experimental and theoretical investigations into the physics associated with the nearly one-dimensional properties of such compounds. Unfortunately, the small sizes of available single crystals and the large anisotropy often combine to produce frustrating experimental difficulties, particularly with respect to measurements of the dc electrical conductivity. The difficulties are most effectively demonstrated by the widely disparate results of the temperature-dependent b-axis conductivity, σ_b, of TTF-TCNQ reported by many laboratories (see summaries in Refs. 3 and 4) and the ensuing effort to resolve the controversy.[5–14]

TTF-TCNQ is a monoclinic crystal[15] which usually grows in the form of nearly rectangular parallelpipeds 2 to 4 mm along the b axis, 0.2 to 0.4 mm along the a axis, and 0.02 to 0.04 mm along the reciprocal-lattice c^* axis. A majority of laboratories, using conventional four-probe techniques,[16] find a room-temperature $\sigma_b(T_r)$ of 300–500 $(\Omega\,\mathrm{cm})^{-1}$ which increases to a maximum 10 to 30 times this value near 58 K, a temperature about 4 K above a metal-to-insulator transition. However, a group at the University of Pennsylvania, while measuring many samples consistent with other laboratories, find a fraction of their samples with exceptionally large conductivities: $\sigma_b(T_r)$ of 660 $(\Omega\,\mathrm{cm})^{-1}$ which rises by a factor of 100 to 150 near 58 K.[4,10]

There have been many attempts to explain the discrepancies on the basis of experimental difficulties. They fall into two classes. Explanations of the first maintain that variable sample purity or defect densities are responsible for the large scatter of peak conductivities and in particular prevent, in most groups, the realization of the largest conductivities as seen at Pennsylvania.[4,10,12] Explanations of the second class take the more common peak σ_b of 20 to 30 times $\sigma_b(T_r)$ as intrinsic and suggest that the measurement of an extraordinarily large peak conductivity is a consequence of the low voltages which might be measured between voltage contacts as a result of the sensitivity, peculiar to anisotropic conductors (as explained in Sec. II A), of the voltage distribution to nonuniform current paths.[6,8,9,14]

The numerous investigations aimed at determining the extent to which the two explanations are operating have employed a variety of approaches, including power-law fits to determine residual resistivity,[7,12,17,18] contactless microwave conductivity experi-

ments,[12,19–22] and a point-contact four-probe method of Montgomery.[10,23] A number of investigations (of which this work is one) have examined specifically the likelihood and possible consequences of inhomogeneous current paths.[6,13,14] Bickford and Kanazawa,[6] using a movable mechanical voltage probe,[24] examined the potential distribution on samples mounted with a variety of silver-paint-contact configurations and found frequently occurring irregularities attributable to spatial variations of contact resistance within a given contact. That inhomogeneous contacts can be responsible for substantial inaccuracies was demonstrated by Schaefer *et al.*,[14] who deliberately misaligned pointlike contacts and obtained unrealistically large values for the peak σ_b, although the temperature dependence of such artificially enhanced peaks differed qualitatively from extraordinary $\sigma_b(T)$ curves.[13,14]

We wished to study further the difficulties encountered in dc measurements of highly anisotropic conductivities in small samples. Irregularities in the potential distribution must be expected to affect any measurement which places fixed electrodes on a sample surface. Therefore, we have employed methods which use *movable* voltage sensors to map the potential distribution. Three types of experiments were carried out: electron-beam-conductivity measurements (EBCOM) of real crystals, conventional movable contact measurements of real crystals, and electrolytic-tank-simulation measurements. We used the mechanical probe to confirm the EBCOM results as well as provide complementary data. The results from the movable beam and contact experiments were used as a guide for modeling inhomogeneous contacts in the electrolytic tank where conventional four-probe measurements of the electrolyte revealed the errors associated with the faulty contacts.

In the EBCOM technique, three leads are fixed to the sample with silver paint: one removes to ground the current injected into the sample by the electron beam of a scanning electron microscope (SEM) and the remaining two measure the *Ohmically* produced voltage which appears between them. For the accelerating voltage employed in this work (2.5 kV), the beam is expected to thermalize within 0.3 μm of the sample surface[25] and can therefore be regarded as a movable surface current electrode. (The method can in principle be used to probe three dimensions by increasing the accelerating voltage and hence the penetration depth.) By a well-known reciprocity theorem,[26] the arrangement is identical to one in which the current passes between the two voltage contacts and the voltage is measured between the third contact and the beam position. The measurement is thus equivalent to the movable-contact method in which one uses a fine wire to sense the potential at various points on the surface of a sample through which current is flowing. The experimental details are given in Sec. III.

We applied both the EBCOM and movable-contact techniques (compared in Sec. II A) to a group of crystals which had been screened for smooth faces and minimal internal flaws and which were mounted with contact geometries appropriate for studying the current flow from the current electrodes in both the four-probe and Montgomery "point-contact" techniques. We find three characteristic anomalies in the potential distributions: (i) those attributable to inhomogeneous contacts (Sec. IV B); (ii) those attributable to fine cracks (Sec. IV C); and (iii) those associated with a topological surface imperfection where the electric field becomes anomalously small (Sec. IV D).

To calculate conductivities, we applied quantitative methods outlined in Sec. II C. These methods work even in the presence of large classes of current flow irregularities. We find average room-temperature values for our samples to be $\sigma_b = 490 \pm 80$ and $\sigma_a = 1.21 \pm 0.15\ (\Omega\,\mathrm{cm})^{-1}$ as discussed in Sec. IV E.

We extended the movable-contact and beam methods to low temperatures. However, considering the difficulites involved, we could more effectively focus on the low-temperature consequences of irregular current flow by modeling imperfections in an isotropic equivalent realized with an electrolytic tank; the results are discussed in Sec. V. The simulation experiments showed that contact inhomogeneities can lead to large scatter in the measured peak conductivities, and in a few cases, to very large peaks with a temperature dependence resembling published extraordinary conductivity curves.

II. EXPERIMENTAL PRINCIPLES

A. Isotropic equivalent

An anisotropic Ohmic crystal can be mapped onto a crystal of isotropic conductivity σ by means of a transformation of coordinates due to van der Pauw.[27] In this work, the transformation is used to "stretch" equipotential patterns measured on TTF-TCNQ crystals into patterns appropriate for an isotropic conductor, where one can more effectively interpret the constant-potential curves; it also serves as the basis for the (isotropic) electrolytic tank simulations. At the same time, the transformation elucidates the sensitivity of anisotropic conductors to errors resulting from imperfect contacts.

For principal axes of the conductivity tensor parallel to the x,y,z axes of the sample, the transformation to the isotropic sample (primed coordinates) is

$$x' = \beta(\sigma/\sigma_{xx})^{1/2}x \ , \quad y' = \beta(\sigma/\sigma_{yy})^{1/2}y \ , \qquad z' = \beta(\sigma/\sigma_{zz})^{1/2}z \ , \quad \sigma = (\sigma_{xx}\sigma_{yy}\sigma_{zz}/\beta^2)^{1/3} \ . \tag{1}$$

Here we have inserted a dimensionless factor β, which is used to scale the isotropic sample to the size of the electrolytic tank. The particular form for σ guarantees the equivalency of the isotropic and anisotropic samples in the sense that equal voltages appear at (x,y,z) and (x',y',z') for the same total current passing through both.

Applied to a room-temperature TTF-TCNQ sample with $\sigma_a = 1.2\ (\Omega\,\mathrm{cm})^{-1}$, $\sigma_b = 480\ (\Omega\,\mathrm{cm})^{-1}$, and $\sigma_{c^*} = 10\ (\Omega\,\mathrm{cm})^{-1}$ (we neglect for the moment that the a and c^* axes are not principal axes of the conductivity tensor), Eqs. (1) map a sample with b-axis length to a-axis width ratio l/w of 10 onto an isotropic equivalent with l/w of 0.5, a ratio which decreases further at lower temperatures as TTF-TCNQ becomes more anisotropic. Such a "short and fat" sample is poorly suited for conventional four-probe measurements because the boundary value problem describing the potential is dominated by the boundary conditions of the contacts themselves; the sample boundaries are too far removed to smooth out current flow irregularities caused by imperfect contacts.

There is an alternative way of viewing the sensitivity of anisotropic conductors to current flow irregularities. Consider a current density which flows in the ab plane with components J_a and J_b. If we define the angle between the current density vector and the b axis as θ_J we can write $\tan\theta_J = J_a/J_b = \sigma_a E_a / \sigma_b E_b = (\sigma_a/\sigma_b)\tan\theta_E$, where θ_E is the angle between the electric field vector and the b axis. Thus a small deviation of the current from the b axis (produced, for example, by a sample imperfection) is magnified into a huge deviation of the electric field when $\sigma_b >> \sigma_a$. (For $\sigma_b/\sigma_a = 400$, θ_J of 1° moves the electric field off axis by 82°.)

B. Principles of EBCOM

The SEM has been widely used to study electrical properties of materials, especially semiconductors.[28–30] Unlike existing methods, EBCOM determines in detail the surface potential distribution produced by current flowing between pairs of contacts in an *Ohmic* conductor.

Figure 1(a) shows schematically the experimental arrangement and the set of x-, y-, z-coordinate axes (parallel, respectively, to the crystal a, b, and c^* axes) used throughout this paper. A voltmeter of input impedance Z_i measures between contacts B and C the voltage $V(\vec{r})$ which is present as a consequence of the current flowing from the point of beam impact $\vec{r}$ to the current removal contact A. Application of a reciprocity theorem produces an equivalent circuit [Fig. 1(b)] which greatly simplifies the interpretation of the measured voltage: The measured voltage $V(\vec{r})$ is that which *would be* present between the beam position and contact A *if* the beam current had flowed between contacts B and C. Thus the electron beam allows us to map out the potential on the sample surface which would result from current flowing between the two extreme contacts B and C.

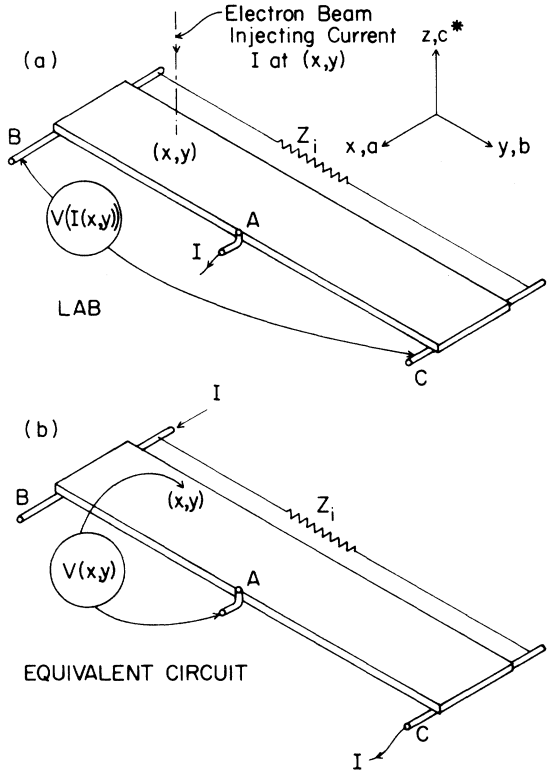

FIG. 1. (a) Laboratory arrangement for the EBCOM experiments. (b) Equivalent circuit obtained by applying reciprocity theorem to (a).

In order to improve the signal-to-noise ratio and to avoid spurious signals caused by the thermoelectric voltages[31,32] which are present from beam heating, the beam position is sinusoidally modulated at frequency f, and the resulting oscillating voltage detected with a lock-in amplifier tuned to f. The voltage presented to the lock-in when the beam is at position $\vec{r}$ is $V(\vec{r} + \vec{a}\cos\omega t)$, where $\vec{a}$ is the amplitude and direction of modulation, and ω is $2\pi f$. For small enough $\vec{a}$, the lock-in output is

$$V_0(\vec{r}) \cong \vec{\nabla} V(\vec{r}) \cdot \vec{a} = -\vec{E}(\vec{r}) \cdot \vec{a} \ . \qquad (2)$$

Thus, the voltage measured by the lock-in is proportional to the component of *electric field* along the modulation direction.

In addition to the electric field, we wish to know the actual potential on the sample surface. In our experiments the potential is determined with an arrangement whereby the beam position $\vec{r}$ is slowly swept along a path s, and the modulation vector $\vec{a}$ is made *parallel* to the path. Under such circumstances, the potential along the path $V(s)$ can be determined

by integrating the measured voltage

$$V(s) = V(0) + \int_0^s \frac{V_0(s)}{a}\, ds \quad . \tag{3}$$

A number of approaches are possible for obtaining the integration constant $V(0)$; we chose the simplest, which is to begin each sweep from a position far removed from the sample, so that $V(0) = 0$ for all sweeps. It can be shown that the integration of the signal over the discontinuity incurred at the sample edge presents no problem for the experimental conditions in this work.[25]

The above discussion assumes that the specimen current is constant throughout the beam sweep. But in fact the current varies with position because of variations in the secondary electron emission and because of limitations in the SEM. Since the voltage on the sample is proportional to specimen current, variations must be corrected for. The correction is accomplished by measuring the specimen current $I(s)$ and defining a corrected potential $\Phi(s)$:

$$\Phi(s) = [I_0/I(s)]\, V(s) \quad . \tag{4}$$

I_0 is a normalization current taken to be 1 A. The spatial derivative of Eq. (4) reveals the required correction to $dV(s)/ds$, the measured electric field

$$\frac{d\Phi(s)}{ds} = \frac{I_0}{I(s)}\left[\frac{dV(s)}{ds} - \frac{V(s)}{I(s)}\frac{dI(s)}{ds}\right] \quad . \tag{5}$$

In practice, two lock-ins are used to measure simultaneously both dV/ds and dI/ds from which, together with their computer determined integrals $V(s)$ and $I(s)$, the corrected quantities $\Phi(s)$ and $d\Phi/ds$ are calculated. The potential and electric field distributions are obtained from the corrected quantities by taking a number of parallel scans over the sample.

C. Determination of σ_a and σ_b from potential distributions

Before discussing the methods by which conductivities σ_a and σ_b are deduced from the potential distribution on our samples, it is important to clarify their relationship to the proper description of the conductivity tensor, which, for monoclinic crystals, generally contains four independent elements.

Ohm's law for a crystalline solid may be expressed in terms of either the second-rank resistivity $\underline{\rho}$ or conductivity $\underline{\sigma}$ tensor

$$\vec{J} = \underline{\sigma} \cdot \vec{E} \quad , \tag{6a}$$

$$\vec{E} = \underline{\sigma}^{-1} \cdot \vec{J} = \underline{\rho} \cdot \vec{J} \quad . \tag{6b}$$

For the moment we concentrate on the description involving the resistivity tensor because its components are more accessible to measurement. As a consequence of irreversible thermodynamics the resistivity tensor is symmetric[33,34]; therefore, there exists a set of three mutually perpendicular principal axes for which the tensor is diagonal. By virtue of the symmetry of the monoclinic Bravais lattice, the b axis is a principal axis, and Ohm's law is of the form

$$(E_x, E_y, E_z) = \begin{pmatrix} \rho_{xx} & 0 & \rho_{xz} \\ 0 & \rho_{yy} & 0 \\ \rho_{xz} & 0 & \rho_{zz} \end{pmatrix} \begin{pmatrix} J_x \\ J_y \\ J_z \end{pmatrix} \quad . \tag{7}$$

Experimental values for the components ρ_{ii} are conventionally obtained by constraining (with a long, thin sample) the current to flow only in one direction and inferring the electric field in that direction by measuring the voltage drop between two points of known separation. For example, ρ_{yy}, the b-axis resistivity (or ρ_b), is found from Eq. (8) to be simply E_y/J_y. Likewise, because $J_z = 0$ in a sample thin in the z direction, the a-axis resistivity ρ_a is

$$\rho_a = E_x/J_x \quad . \tag{8}$$

In the literature, a quantity σ_a is reported, and is defined by the relationship between the measured quantities J_x and E_x:

$$J_x = \sigma_a E_x \quad . \tag{9}$$

Comparing Eqs. (8) and (9), we see that $\sigma_a = 1/\rho_a$, the inverse of ρ_{xx}, a diagonal element of the resistivity tensor. However, σ_a is *not* an element of the conductivity tensor as is evident by solving Eq. (6b) for the resistivity element ρ_{xx} in terms of elements of the conductivity tensor

$$\rho_a = \rho_{xx} = [\sigma_{xx} - (\sigma_{xz})^2/\sigma_{zz}]^{-1} = \sigma_a^{-1} \quad . \tag{10}$$

Because our samples were thin [the condition under which Eq. (9) is a valid definition] we will follow the literature and describe our results in terms of σ_a.

The schemes which are usually used to determine elements of the conductivity tensor,[24,27,35–38] $\underline{\sigma}$, are difficult to apply to TTF-TCNQ because two of the principal axes of $\underline{\sigma}$ are unknown and because crystals are too small and fragile to be sectioned into various orientations. Consequently, we have developed simple methods which allow a determination of σ_a and σ_b from a knowledge of the surface potential distribution in thin crystals. We have not undertaken a measurement of σ_{c^*} because of our crystals' thinness in this direction.

There are two methods by which σ_b may be determined. Both methods are based on the reciprocity equivalent circuits drawn in Fig. 2(a). Current leads are attached to both ends of a sample so that the total current I must pass through an xz cross section perpendicular to the y axis. We specify the y component of the current density by $J_y(x,y,z)$, the y component of the electric field by $E_y(x,y,z)$, and the po-

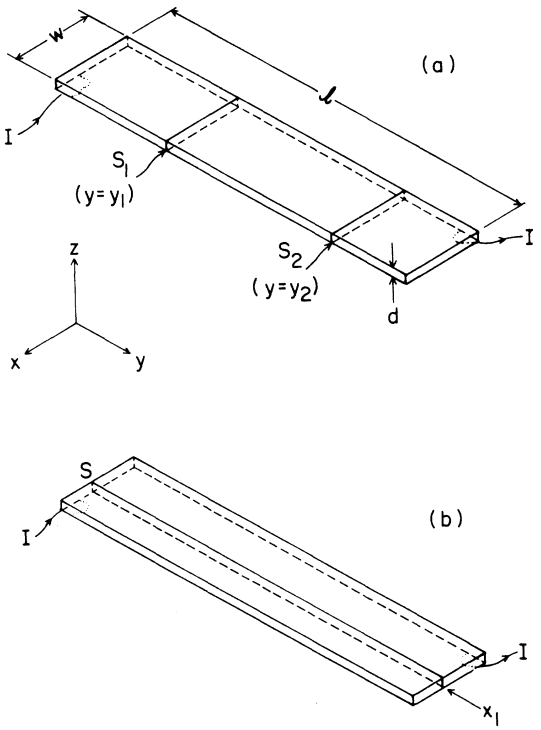

FIG. 2. Geometry for computing conductivities from the potential distribution on the top surface. Current is injected through contacts indicated by dotted lines. (a) Sample and cross sections, S_1 and S_2, appropriate for computing $\sigma_{yy}=\sigma_b$. (b) Sample and cross section S appropriate for calculating $\sigma_a=\rho_{xx}^{-1}$.

tential by $\Phi(x,y,z)$.

The first method requires that there exists an xz cross section S_1 at some y_1, over which $J_y(x,y_1,z)$ is independent of z (an assumption verified in the electrolytic tank) and the conductivity σ_{yy} is homogeneous. (The cross section is not truly rectangular in real crystals, but trapezoidal. Since the crystals are quite thin, we expect that the error introduced by approximating the cross section with a rectangle will be negligible.) By the definition of current density, we have

$$I=\int_0^d\int_0^x J_y(x,y_1,z)\,dx\,dz \quad . \tag{11}$$

Substituting for J_y from Ohm's law [Eq. (6a)] and assuming J_y is independent of z and σ_{yy} is homogeneous, one can obtain σ_{yy} in terms of the experimentally measured E_y:

$$\sigma_{yy}=\left[d\int_0^w E_y(x,y_1,d)\,dx\right]^{-1} \quad . \tag{12}$$

We recall that σ_{yy} is along a principal axis, the b axis, and so $\sigma_{yy}=\sigma_b$.

The second method is also depicted in Fig. 2(a). It requires that there exists a second surface S_2, located at y_2, where the assumptions for S_1 hold. In addition, it requires that σ_{yy} be homogeneous between the two surfaces. Integrating both sides of Eq. (11) over y between y_1 and y_2 gives

$$(y_2-y_1)I=\sigma_{yy}d\int_{y_1}^{y_2}\int_0^w E_y(x,y,d)\,dx\,dy \quad , \tag{13}$$

where the integration on the left has been carried out reflecting the independence of I on y. Exchanging the order of integration and rearranging gives

$$\sigma_{yy}=(y_2-y_1)I\left[d\int_0^w[\Phi(x,y_2,d)-\Phi(x,y_1,d)]\,dx\right]^{-1} . \tag{14}$$

This is the same expression used for calculating conductivity from a conventional four-probe measurement, but with the potential difference between the two voltage electrodes located at y_1,y_2 replaced by the difference in the *average* potential at each electrode site. Equation (14) does not require that the current density be uniform throughout the sample thickness between the surfaces S_1 and S_2. In addition, it holds even in the presence of thin cracks which possess the property that no line parallel to the y axis intersects the crack at a nonzero angle. [See Ref. 25 for methods whereby the denominators of Eqs. (12) and (14) are measured *directly*.]

σ_a is obtained by arguments similar to those leading to Eq. (12) but applied to the cross section of Fig. 2(b):

$$\sigma_a=\rho_{xx}^{-1}=l/d\int_0^l E_x(x_1,y,d)\,dy \quad . \tag{15}$$

III. EXPERIMENTAL

A. Apparatus

For our experiment, the conventional organization[39] of the SEM (JEOLCO Model JSM U-3) was modified as depicted in the block diagram of Fig. 3. To reduce possible radiation damage and beam heating, the accelerating voltage was decreased to 2.5 kV with an external supply. The decrease required substituting for the standard magnetic-lens control circuits a simple power supply and series resistor network.

For most experiments the entire SEM sample stage was replaced by one which could rotate 360° about a horizontal axis and which used an Air Products, Inc. "Heli-tran" to reach low temperatures. A Princeton Applied Research Corporation temperature controller, using a GaAs diode sensor, stabilized temperaturre to ±0.1 K. The temperature was measured with a potentiometer reading a Chromel P vs Au-0.07-at.% Fe thermocouple referenced to an ice junction. A guard ring biased at +300 V to ground was fixed over the sample to collect secondaries and prevent their return to the sample and the current

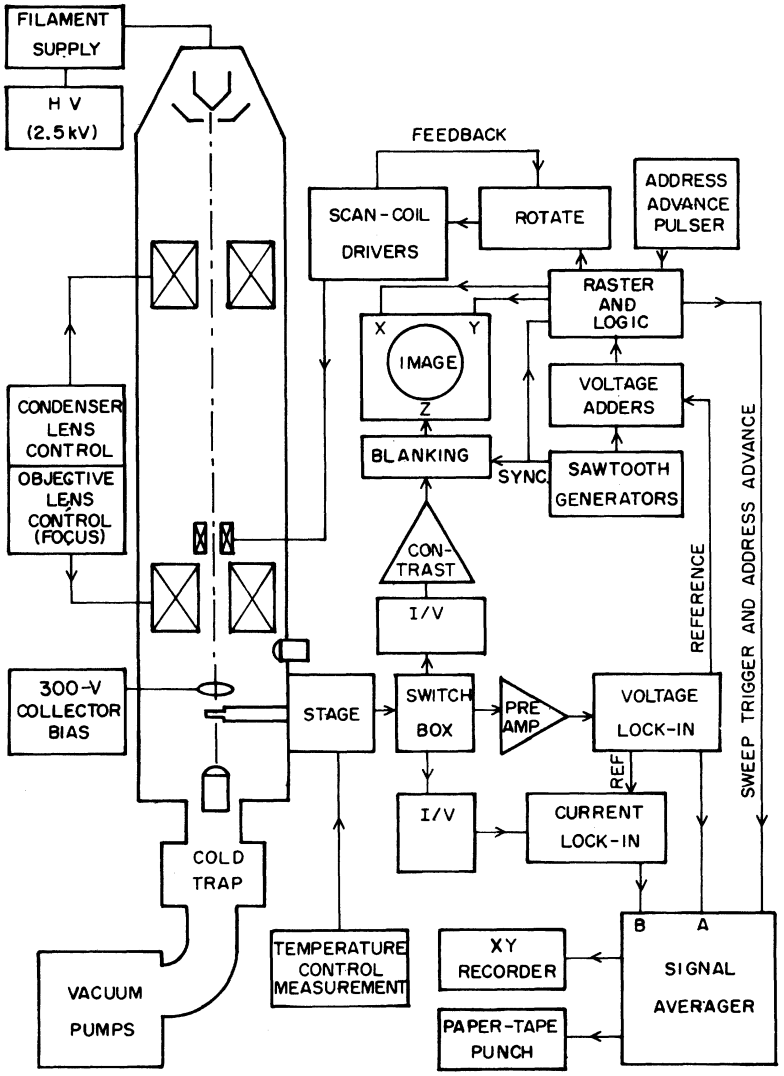

FIG. 3. Block diagram for EBCOM experiment.

detection circuitry. (The secondary current represented about 50% of the total beam current for a 2.5-kV beam.)

The standard waveform generators were switched out of the circuit so that the beam sweep could be externally controlled. The scan control voltage, produced by adding appropriate waveforms, together with associated synchronization pulses were presented to a digital raster generator, the output of which was applied to a rotate circuit. The rotate circuit was responsible for orienting the scans of the raster to be parallel to the desired direction on the crystal, which, once mounted on the cryogenic stage, could not be rotated about the beam axis. Finally, scan voltages were applied to the SEM scan coil drivers; overall current feedback assured that the magnetic deflection fields followed the applied scan control voltages.

We refer to the circuitry responsible for detecting the voltage and current derivative signals as the voltage arm and current arm, respectively. The detection circuitry was routed with a switch box to the desired contacts on the sample. The voltage arm consists of a low-noise battery-operated preamplifier, a lock-in amplifier, and half of the signal-averager memory. The preamplifier utilized parallel input transistors[40] to achieve a gain of 230 and a noise figure of 2 dB for a 20-Ω source resistance over a frequency range of 1 to 10 kHz. The preamplifier output was presented to the differential inputs of a Princeton Applied Research HR-8 lock-in amplifier which operated typically with a 1-msec time constant and a voltage gain of 5×10^5. The voltage-arm lock-in also supplied the scan circuitry and the current lock-in with a 10-kHz reference signal.[41] The output

of the lock-in was connected to the A channel of a Nicolet 1072 signal averager which stored the different scans of a given data set sequentially in one-half of its memory.

In the current arm, a two stage current-to-voltage circuit converted specimen current to a voltage signal and provided separate outputs with sensitivities of 50 μV/nA and 2 mV/nA. The second stage signal was sent to the contrast amplifier for imaging the sample with the specimen current; the first stage was routed to the current lock-in operating with gain of 10^4. The detected voltage, proportional to dI/dx, was finally presented to the B input of the signal averager, where it was multiplexed into the second half of the memory. The total averager memory of 1024 channels led to a resolution of about 1.3% of the swept sample dimension. Accumulated data were finally recorded on an xy recorder and read out on paper tape for computer processing.

B. Experimental methods

Single crystals of TTF-TCNQ were solution grown in distilled acetonitrile[42] from starting materials which had been twice recrystallized and subsequently purified by two or threefold gradient sublimation. Crystals free from surface flaws (less than 1% of the yield) were chosen and mounted over copper sample holders in two kinds of contact configurations, which we hereafter refer to as the "extended" and "point" contact arrangements. In the extended arrangement, two voltage measuring leads, which also serve to support the sample, run across the width of the bottom face at opposite ends of the sample as illustrated in Fig. 1. A third electrode for current removal is attached with as small a contact as possible to an edge of the sample midway between the ends. By the reciprocity theorem, the extended configuration is appropriate for studying the potential distribution which would be produced by the current electrodes alone in a four-probe measurement of the b-axis conductivity. In the second, point-contact, arrangement, the sample is supported by two electrically insulated wires and has three leads attached to three corners of the bottom face with as small a contact area as possible. (In practice, the contact diameter was about 25% of the sample width.) By switching among the leads, it is possible to investigate in the reciprocity equivalent, three different cases of current flow: "transverse," when current electrodes lie on the a axis; "longitudinal," when on the b axis; "diagonal," when on diagonally opposite corners. The diagonal arrangement is of particular interest because with it, the methods of Sec. II C allow *both* σ_b and σ_a to be measured; however, for σ_b in excess of 10^3 $(\Omega\,\mathrm{cm})^{-1}$, it turns out, for the sample thicknesses and specimen currents employed, that the longitudinal arrangement should be used to measure σ_b because of the better signal-to-noise ratio.

The 0.001-in. gold leads were connected to the sample either with DuPont Corp. 7431 silver paint thinned with butylcellosolve, or with a conductive mixture of Duco Cement (DuPont) and silver powder (80:20 ratio by weight) thinned with butylcellosolve.

Data acquisition was obtained with 5–10-nA specimen currents focused into a spot 6 to 8 μm in diameter. Modulation, always applied parallel to the scan direction, had an amplitude adjusted to be 5% of the sample dimension parallel to which the beam was to be scanned.

The scanning was controlled by the raster-logic circuitry in the following manner. Beginning at (x_0,y_1), a position well removed from the sample, the beam was scanned with a linear ramp (0.1–0.3 sec/scan) along x completely across the sample and off the opposite side. It was then returned to a position (x_0,y_2) and scanned again. Scanning continued through the final sweep beginning at (x_0,y_4) after which the entire process was repeated; in this manner data were acquired over a loose raster pattern on the sample. Typically, 4000 repetitions taking about one hour constituted a given data set, but this number and time depended on the signal-to-noise ratio for the crystal under study (rms signal voltage to rms noise voltage was typically 1:9 before averaging). One to three additional data sets per sample were obtained by shifting the position of the whole raster. Samples with the extended-contact geometry were studied with scans parallel to the b axis, called longitudinal scans, while point-contact samples were swept across their width (along the a axis), called transverse scans.

The registry between the raster scans and the actual sample coordinates was recorded by double exposing on film the specimen current derived image of the sample and an image produced by the raster pattern itself.

Sample dimensions were measured from SEM or optical micrographs. Dimensions were measured from the micrographs with a digital recording device which displayed the coordinates of a movable cross hair. This device also provided punched cards so that sample features could be plotted by computer, along with equipotential patterns. The uncertainty of the length and width dimensions is less than 2%, while the sample thickness is known to $\pm 5\%$.

C. Representative results of EBCOM

Representative data and computer-corrected results for a *single* longitudinal scan on sample No. 1, an extended-contact sample, are shown in Fig. 4. The data were obtained from 8200 repetitions each lasting 0.102 sec. The large peaks in the derivative data

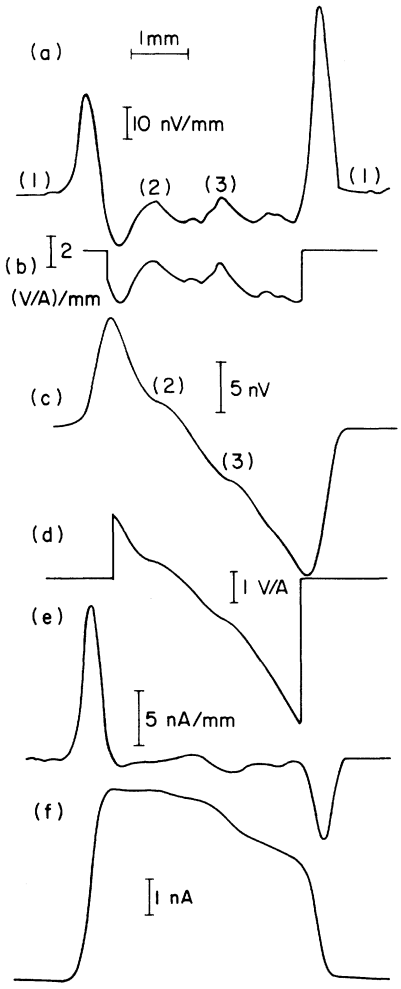

FIG. 4. Representative EBCOM data for a scan along the *b* axis on sample No. 1. (a) Voltage derivative signal; (b) after correction for current variations and normalized to 1 A; (c) integral of voltage derivative; (d) Φ, the corrected potential; (e) current derivative signal; and (f) its integral.

[Figs. 4(a) and 4(e)] occur when the modulation is straddling the edge of the sample. (Theoretical line shapes for the voltage derivative data are given in Ref. 25.) The noise level in the derivative data can be ascertained from regions (1) in Fig. 4(a), where the beam is entirely off the sample. In the same curve, there are two regions, labeled (2) and (3), where the electric field becomes small. These regions correspond to the plateaus seen at locations (2) and (3) in the integrated voltage curve, Fig. 4(c). (The plateaus are also found at the same positions in six of the remaining seven scans for this sample.) Plateaus for this and other samples are discussed in Sec. IV D.

The noise in the current-arm signal is negligible. The variation in the specimen current, here worse than usual, is attributable in largest part to the dependence of the beam current on beam deflection.

The electric field and potential, corrected for current variations, are shown in Figs. 4(b) and 4(d). The corrected curves are cut off before the sample edges because small alignment errors make accurate corrections of the rapidly varying edge signals difficult to achieve.

Finally, we present in Fig. 5 equipotential plots derived from the corrected potential of eight longitudinal scans. Figure 5(b) is a scale drawing of sample No. 1 with equipotentials superimposed. The contacts, which are attached on the underside of the sample, are indicated by dashed lines. Also displayed are the excursion of the peak-to-peak modulation, the distance corresponding to the rise time of the lock-in time constant, and the uncertainty in registration estimated to be ± 1 address of the signal

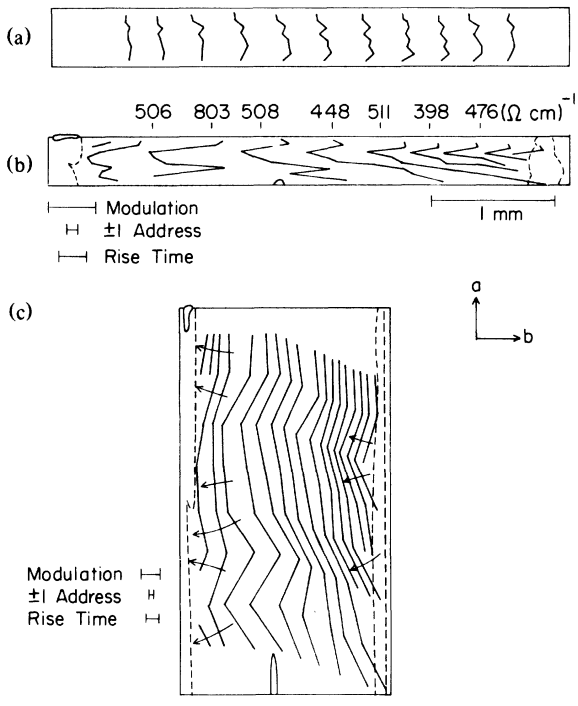

FIG. 5. (a) EBCOM equipotential pattern on the top face of a sample of amorphous graphite. Silver paint contacts are at ends of sample on bottom face. Potential interval is 0.47 V/A. Sample dimensions are $3.511 \times 0.399 \times 0.025$ mm. (b) EBCOM equipotential pattern on the top *ab* face of sample No. 1. Potential interval is 0.77 V/A. The conductivities determined at various places on the sample are indicated. Sample dimensions are $4.151 \times 0.366 \times 0.041$ mm. (c) Isotropic equivalent assuming $\sigma_b/\sigma_a = 400$. Potential interval is 0.39 V/A. Arrows indicate approximate current-flow direction.

averager memory. For comparison, we display in Fig. 5(a) an EBCOM equipotential pattern for a sample of graphite, mounted with silver paint contacts just as sample No. 1. The striking deviations in the sample No. 1 pattern are more usefully displayed by mapping the equipotential pattern onto an approximate isotropic equivalent sample as is done in Fig. 5(c).

On the right-hand side of the sample the equipotentials show that more current was injected in the upper half of the sample than the lower. This current spreads out and flows irregularly into the left contact. Some silver paint, which had flowed up over the top of the sample during mounting (in the upper-left-hand corner), appears to be acting as a current sink. Note that along any line where a four-probe voltage electrode might be situated, the potential is not constant.

The spacing between equipotentials increases on the average in the left-hand half of the sample. Although due in part to the plateau in potential and to some degree to a more uniform current distribution on the left, the rarefied spacing is primarily accounted for by an increase of the sample thickness from 28 μm on the right to 43 μm on the left. (Such a large variation of sample thickness is atypical.)

To obtain σ_b, the data were analyzed by Eq. (12). The results vary depending on where the cross section is placed. By displaying the conductivity along with the equipotential pattern, a sharp enhancement can be seen to occur at the location of a potential plateau. There are a number of factors which contribute to the overall variation of the calculated σ_b. Noise is expected to account for most of the variation ($\pm 10\%$). There is a significant region in the upper-right-hand corner where no data exist. Since in this region the electric field was assumed constant and equal to the value occurring in the densely packed area directly below, the conductivity could be underestimated here. Finally, the conductivity itself may be inhomogeneous.

An average of 63 equally spaced cross sections gives $\sigma_b = 502 \pm 131\ (\Omega\,\mathrm{cm})^{-1}$ where the uncertainty represents the standard deviation about the mean. As we discuss in Sec. IV D, however, the large conductivities associated with the potential plateaus are probably spurious; if we omit these regions, the mean conductivity becomes $460 \pm 52\ (\Omega\,\mathrm{cm})^{-1}$.

D. Mechanical-probe technique

In the usual movable-contact approach,[6,24] a mechanically positioned probe is used to sense the voltage on the surface of a sample through which current is flowing. We obtained identical information by applying the reciprocity theorem and maintaining the same lead configuration as in the SEM; that is, we fed ac current to the sample through the mechanical probe itself and used one of the three leads fixed to the sample for current removal and the other two for voltage measurement. The reciprocity theorem was verified by comparing, on one sample, data obtained with both the conventional and our arrangement; the potential distributions coincided to within our spatial resolution and σ_b agreed to within 1.5%.

Samples were mounted on the same cryogenic stage used for the SEM measurements; a vacuum chamber mated with the stage so that measurements could be extended to low temperatures. The chamber was equipped with a window through which the sample could be observed with a reticle outfitted microscope. The probe consisted of a 0.001-in. gold wire 5 mm long attached to an arm which could be positioned through a bellows with a micromanipulator situated outside the vacuum chamber. The tip of the wire which was to contact the sample was flattened, cut with a razor blade to the shape of a fine edge, and coated with mercury to decrease contact resistance.[6] The coordinates of the probe could be determined to about ± 15 μm. Current at 400 Hz was developed by up to 100 V supplying a 10-MΩ series resistor. The current and voltage were detected simultaneously with two lock-in amplifiers.

The mechanical-probe method, unlike our application of EBCOM, was relatively free from problems associated with signal-to-noise ratio because it enjoyed three to four orders of magnitude more specimen current. Because our method is an ac technique, dc thermopower potentials arising from temperature gradients present no problem (ac temperature gradients generated by Joule heating in the probe-sample contact resistance occur at twice the reference frequency and escape detection).

Although the probe-sample contact resistance was typically less than 10 kΩ, it could become comparable to the 10-MΩ impedance of the current source and thus decrease the current. Because *both* the voltage and current were measured, such current variations could be accounted for. Nonetheless, the problem of maintaining electrical continuity was compounded at low temperature because mercury could not be applied and slight condensation on the sample from the relatively dirty vacuum (10^{-5} Torr) electrically insulated the surface. Successful contact was generally unpredictable, and only one sample produced useful low-temperature data with the mechanical probe. (Although a cleaner vacuum system would alleviate the insulating condensation, we note that probe-to-sample resistance problems are *completely* eliminated by EBCOM.)

IV. RESULTS

We investigated a total of ten TTF-TCNQ samples, five mounted with extended contacts and five with

point contacts. Of the extended contact samples, three were studied exclusively with EBCOM, one with the mechanical probe, and one with both methods. Of the point-contact samples, three were studied exclusively with the mechanical probe while the remaining two were investigated with both techniques. Measurements on four samples were extended to lower temperatures, three with EBCOM and one in the movable contact apparatus. The use of two movable-sensor techniques has enabled us to (i) verify the validity of the EBCOM (Sec. IV A); (ii) identify *directly* the problems which can occur in conventional four-probe measurements on TTF-TCNQ samples (Secs. IV B–IV D); (iii) obtain the room-temperature conductivities σ_a and σ_b independently of current-flow problems (Sec. IV E); and (iv) demonstrate that both movable beam and probe experiments can be extended to low temperatures. In regard to (ii) above, it is important to note that while for the most part TTF-TCNQ crystals may be regarded as a two-dimensional problem, crack-induced potential distortions (Sec. IV C) and potential plateaus (Sec. IV D) are in fact a consequence of the problem being three dimensional.

A. EBCOM and mechanical-contact comparison

An irrefutable test for the validity of EBCOM is provided by a comparison with the results of the movable pressure-contact technique. Three samples were therefore first studied with the mechanical probe and then transferred to the SEM for EBCOM measurements.

The comparison of the potential distributions is provided in Figs. 6 and 7, which depict, respectively, the equipotential patterns for an extended-contact sample No. 2 and a point-contact sample No. 10. Figures 6 and 7 demonstrate that both techniques are recording essentially the same equipotential patterns. At the same time they provide a basis for the following comparison of the relative merits of the two techniques as regards their ability to record potential distributions.

EBCOM generally produces less smooth plots for a number of reasons. First, the noise in the potential causes some scatter. Second, registration of data with the sample coordinates is more difficult in the SEM: the location of the sample edge is inferred from the current signal and is subject to at least ± 1 address of the signal averager memory. Third, the data are shifted along the scan direction because of the rise time of the lock-in time constant. When sweeps are taken in the same direction (as they were for most of our data), these shifts appear as a systematic displacement; for sample No. 2, however (Fig. 6), sweeps were made in alternating directions, which required a correction for the alternating rise-time shifts. Fourth, errors in determining the zero in the voltage-arm data of any given scan are integrated to give a linearly rising or falling baseline in the potential which acts as voltage displacement with respect to other scans. (Such errors are minimized by adjusting the zero of the raw derivative data until its integral

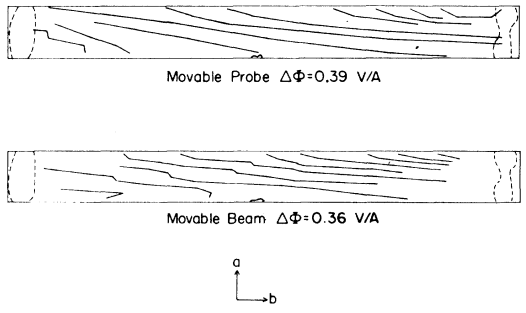

FIG. 6. Comparison of EBCOM and mechanical-contact equipotential patterns on sample No. 2. Two contacts are on bottom face as indicated with dashed lines; the third is on the lower edge in the middle of the sample as indicated. Sample dimensions are $4.799 \times 0.509 \times 0.087$ mm.

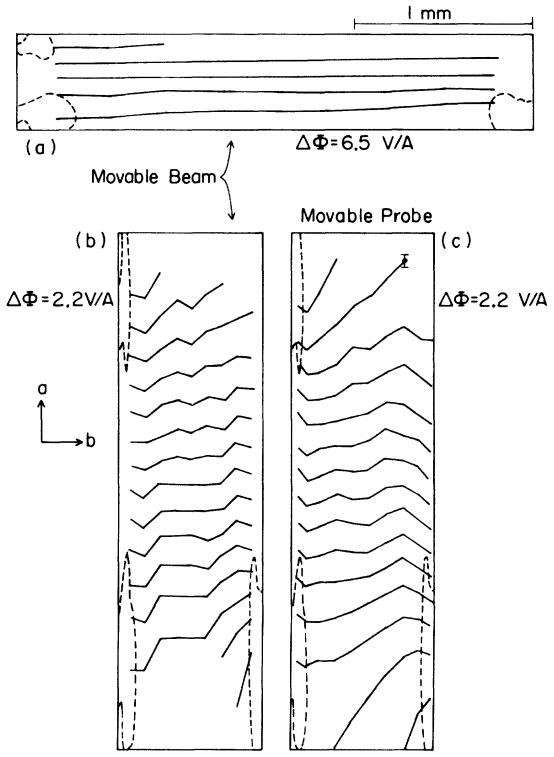

FIG. 7. Equipotentials obtained on sample No. 10 with EBCOM (a) and (b), and mechanical probe (c). Current flows between diagonal contacts in reciprocity equivalent sense. (b) and (c) Isotropic equivalents assuming $\sigma_b/\sigma_a = 400$. Sample dimensions are $2.895 \times 0.534 \times 0.39$ mm.

TABLE I. Room-temperature-conductivity results, where method I uses Eq. (2.12) and method II, Eq. (2.14).

Sample No.	Technique	σ_b $(\Omega\,\mathrm{cm})^{-1}$	Method	σ_a $(\Omega\,\mathrm{cm})^{-1}$	Method
Extended contacts					
1	EBCOM	460 ± 56	I[a]		
2	EBCOM	521	I[b]		
	PROBE	429 ± 62	I		
3	EBCOM	405 ± 67	I[a]		
4	EBCOM	530	I[b]		
5	EBCOM[c]	499 ± 35	I	1.38	I
	PROBE	586 ± 87	I	1.12 ± 0.06	I
6	PROBE	482 ± 18	II		
Point contacts					
7	PROBE[c]	634 ± 20	II	1.42	I
	PROBE[d]			1.53	I
8	PROBE[c]			1.13 ± 0.03	I
	PROBE[d]	463 ± 56	I		
	PROBE[e]	455 ± 78	II	1.08	I
9	PROBE[c]	428 ± 49	I	1.15	I
		432 ± 85	II		
10	PROBE[c]	332 ± 41	I	1.12 ± 0.07	I
	EBCOM[c]	439 ± 149	I	1.11 ± 0.03	I

[a]Omitting plateau regions.
[b]Using least-squares slopes of potential curves for electric field.
[c]Transverse contact configuration defined in Sec. III B.
[d]Longitudinal contact configuration defined in Sec. III B.
[e]Diagonal contact configuration defined in Sec. III B.

starts from and returns to zero.)

The relative spatial resolution of the movable contact and beam techniques is an important consideration. The resolution *along* the scan for EBCOM is of the order of the modulation amplitude. This prevents, for example, the determination of the potential within a modulation amplitude of the sample edge over which the beam is scanned. On the other hand, the EBCOM automatically obtains data continuously over a scan, while the mechanical probe, without complicated mechanical movements, acquires data at discrete points, the spacing of which is limited by the patience of the operator. The importance of continuous acquisition is exemplified by the discovery of the potential plateaus. Finally, the resolution perpendicular to the scan direction in the SEM is simply the beam radius, which for our experiments was about 4 μm, while for the mechanical probe it is the radius of the wire contact, about 8 μm in our experiments. The resolution in the SEM was sufficient for most of the purposes of our experiments, but future applications of EBCOM could make use of very fine spot diameters (less than 1000 Å) which can be routinely achieved in modern electron-optical systems.

The quantitative verification of EBCOM is provided by comparison between the EBCOM and mechanical contact conductivities of sample Nos. 2, 5, and 10 tabulated in Table I. σ_b for sample No. 10 is presented for purposes of intertechnique comparison only, since the potential distribution exhibited peculiarities which were later linked to a cleavage crack separating the top and bottom of the sample: the b-axis result is therefore unreliable. The uncertainties listed for σ_b are standard deviations about the mean of a number of determinations [using Eq. (12)] taken at different locations on the sample. (The large uncertainty for sample No. 10 is probably related to the severity of the cleavage.) Because the point-contact configuration was used for sample Nos. 5 and 10, σ_a could also be determined, and the two techniques can be seen to be in satisfactory concordance.

B. Contact inhomogeneities

We have found that nonuniform contact resistance is the most common source of two-dimensional current-flow irregularity. Such nonidealities are in greatest evidence for the extended contacts, in which nonuniformities can cause irregular potential distributions to extend over the entire length of sample. For example, the equipotential pattern for sample 1 (Fig.

5) shows that current was injected and removed nonuniformly along each electrode length. It must be stressed that under microscopic examination the contacts appeared quite uniform: the silver paint had flowed freely and smoothly from the lead onto the sample.

An explicit demonstration of the nonuniform contact resistance responsible for irregular current injection is provided by the potential distribution for the point-contact sample 8. Figure 8 shows the equipotentials obtained with the mechanical contact for a longitudinal-contact configuration. Electrolytic tank data show that directly above the contacts the equipotential pattern should nearly mirror the contact shape, certainly not the case here. In particular, the potential distribution above the upper-right-hand contact shows that nearly all of the current was injected into the sample from the center of the contact area. The contact resistance for this contact (45 Ω) was less than many of the point contacts which suggests that the magnitude of contact resistance is a misleading test of quality: an unusually low resistance may indicate excellent electrical continuity at only a few places over a contact surface. The result for this sample confirm *directly* that spatially inhomogeneous interfacial contact resistance is playing a role in the potential distribution and supports the conclusions which Bickford and Kanazawa[6] inferred from their equipotential data.

In one of our extended contact samples, No. 6, the equipotential pattern was found to be very well behaved and is shown in Fig. 9. For this sample, silver paint was allowed to flow completely around the crystal ends so that each contact capped the crystal ends and covered about $\frac{1}{4}$ of the sample length. The third electrode was spread entirely across the sample width on the bottom face. The average conductance per unit area of contact-sample interface was comparable to our other samples (about 2 Ω^{-1}/mm^2). It would be useful to know if the uniform current flow associated with this sample is a consequence of silver paint capping the crystal ends and edges, or if it is simply a result of an increased number of low resistance areas occurring over the large electrode area on the *ab* faces. Further experiments would be needed to resolve such questions, but we note that the potential distribution for sample 6 is consistent with the assumption that the probability per unit contact area of making a low resistance path is a constant for edges, ends and *ab* faces, and that the uniform current flow is then simply a consequence of the large contact area on the *ab* faces. It would seem that making the contact area as large as possible in order to increase the number of low resistance paths between silver paint and sample is desirable but not foolproof: Bickford and Kanazawa showed that simply wrapping paint around the crystal ends is no guarantee that current will be uniformly injected.

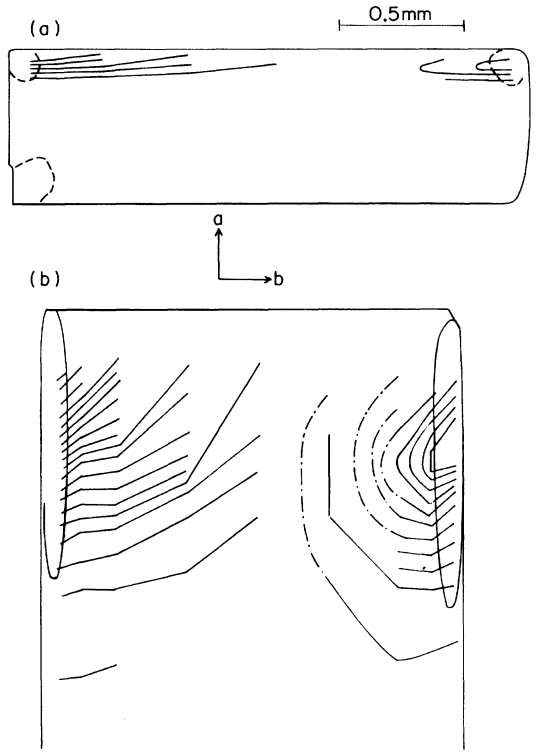

FIG. 8. Equipotential patterns for the top *ab* face of sample No. 8 obtained with mechanical probe. Silver paint contacts are on the bottom *ab* face as indicated. Sample dimensions are 7.041 × 0.611 × 0.049 mm. (a) Equipotential spacing is 0.95 V/A. (b) Detail of sample and equipotential pattern in the isotropic equivalent. Dot-dash curves are extrapolations. Equipotential spacing is 0.315 V/A.

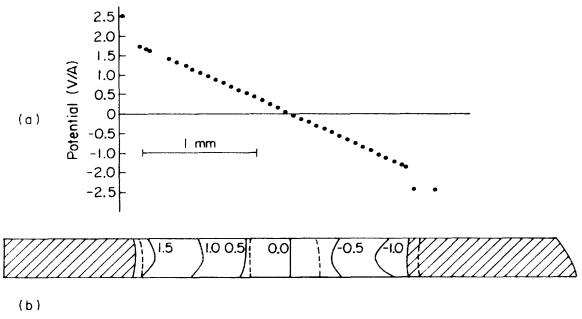

FIG. 9. Mechanical-probe results for sample No. 6 which had large silver paint contacts capping the ends of the crystal. (a) Potential normalized to 1 A on the top surface along a path in the middle of the sample width. (b) Equipotential pattern. Third contact is on bottom face as indicated by dashed lines. Extent of the end contacts on bottom surface is also shown by dashed lines.

Given an irregular potential distribution, nonuniformities of the interfacial contact resistance in the voltage measuring contacts leads to erroneous measurements in the following manner. Regard the voltage electrode as a set of N discrete parallel resistors R_i, linking a lead to various places on the sample. The voltage appearing on the lead will be

$$V = R_p \sum_{i=1}^{N} \frac{V_i}{R_i} , \tag{16}$$

where R_p is the parallel resistance of the R_i, and V_i is the voltage present on the sample at the point of contact of R_i. The voltage electrode thus measures a weighted average. (If the R_i are small enough, voltage electrodes make current flow more uniform by shorting out potential differences across the width of the sample. In light of the nonuniform potential measured over the current electrodes, however, such shorting should not generally be expected.) Note that if the average represents a random and finely enough distributed sampling over the electrode area, then by Eq. (14) no error will be incurred in the measurement, as long as current is flowing uniformly throughout the sample thickness. An electrolytic tank study of the effect of inhomogeneous current and voltage electrodes on four-probe measurements is presented in Sec. V.

C. Sample cracks

Although samples were carefully selected, small imperfections in the form of planar cracks were unavoidably present in a number of them. Our studies included careful examinations with reflection and transmission optical microscopy and electron microscopy, as well as the potential distribution measurements, and provide evidence of the following: (a) the distortion of potential which a crack induces is strongly dependent on its orientation with respect both to the direction of current flow and to the direction of high conductivity; (b) some cracks behave as if they formed incomplete breaks such that current paths passed through their plane; and (c) a crack-induced distortion of potential changes with temperature.

The potential distributions obtained by mechanical probe for sample 9 are shown in Fig. 10 and illustrate a relative immunity to cracks when $\vec{J}$ (here flowing between diagonal contacts) has an a-axis component. Optical micrographs indicated that imperfections existed in the bulk primarily in the left two-thirds of the sample. The lack of evident distortion is probably a consequence of the large σ_b/σ_a anisotropy as discussed in Sec. II A; i.e., even a small a-axis component to $\vec{J}$ causes $\vec{E}$ to lie nearly parallel to a such that further deviations in $\vec{J}$ caused by cracks only slightly affect the direction of $\vec{E}$. Electrolytic tank experiments show this is especially true if the cracks are partially conducting or do not intersect both top and bottom surfaces.

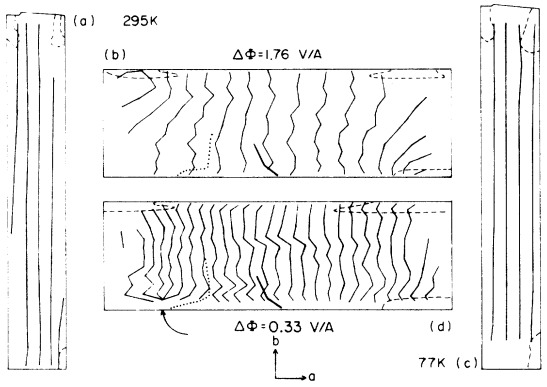

FIG. 10. Equipotential patterns obtained with the mechanical probe on the top face of sample No. 9. Two cracks intersecting top and bottom surfaces are shown as heavy and dotted lines, respectively. Patterns (a) and (b) are at room temperature, with potential intervals of 5.28 and 1.76 V/A, respectively. Patterns (c) and (d) are at 77 K, with potential intervals of 1.99 and 0.33 V/A. (b) Room-temperature isotropic equivalent; (d) stretched by same amount, inappropriate for σ_b/σ_b at 77 K. Contacts were repainted before the low-temperature work.

At 77 K, however, a number of constant potential curves converge to a point [see arrow Fig. 10(d)] lying on a crack visible in transmitted light. The crack became a more severe perturbation, possibly because its resistance relative to the surrounding material increased at lower temperature.

When viewed along an edge, TTF-TCNQ crystals exhibit a laminar structure, with individual laminae lying parallel to the *ab* faces. Because the crystals cleave along these (001) planes, it might be expected that separation of the laminae may occur. In fact, indirect evidence for this has been reported.[7,43] One of our samples, No. 10, *which appeared above average under a stereo microscope,* exhibited directly that such a crack can distort the three-dimensional current flow. Its potential distribution was obtained with EBCOM on both the top and bottom faces for current point-contacts place (in the reciprocity equivalent sense) along a common b-axis edge. Figures 11(c) and 11(d) represent the equipotential pattern on the bottom surface viewed as if sighting down through the crystal from above. Dashed lines outline the contacts, while dot-dash lines are extrapolations of constant potentials. Qualitatively, the bottom-face equipotential pattern shows that current is flowing primarily along the b direction between contacts as expected. In Figs. 11(a) and 11(b), however, the equipotentials for the top surface bear no resemblance to the expected pattern. Subsequent to the measurements, it was discovered that the crystal was separated by a plane cleavage crack, parallel to the *ab* faces,

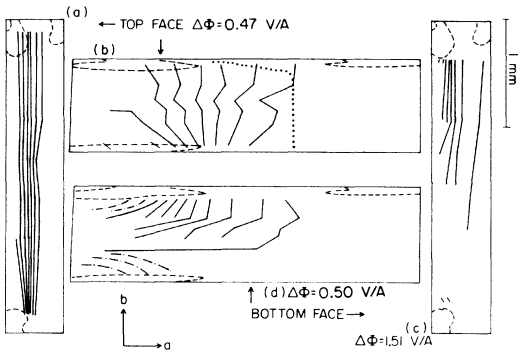

FIG. 11. EBCOM equipotential patterns for sample No. 10; sample dimensions are 2.895 × 0.534 × 0.039 mm. (a) Scale drawing of sample; equipotential pattern on top face. (b) Isotropic equivalent assuming $\sigma_b/\sigma_a = 400$. The dotted line indicates the right-hand limit of a crack which separated the top of the sample from the bottom. (c) Scale drawing; equipotentials on bottom face. (d) Same as (c) except width expanded 20 times.

which extended from the left-hand edge until it terminated along the curve indicated by the dotted line in Fig. 11(b).

In contrast to the large distortion described above for current flowing between longitudinally placed contacts, the potential distribution for diagonal current flow (Fig. 7) was only slightly modified by the presence of the cleavage. The electric field in the middle region of the sample gave values for σ_a in agreement with reported values,[10] even at 45 and 62 K. Evidently, the resistance for current paths through or around the cleavage was of such a magnitude, compared to the resistance between diagonal contacts (about 33 Ω at T_r) that current was able to reach the top half of the crystal.

D. Potential plateaus

In all those extended contact samples studied with EBCOM we found regions, extending entirely across the sample width, where the potential as a function of the coordinate along the b axis leveled off to form a plateau, as seen, for example, in Fig. 4. In every case (two plateaus in sample No. 1, two in No. 2, one each in Nos. 3 and 4) the location of the plateau coincided with a subtle surface feature to be described below.

In the two samples which exhibited plateaus and for which data were also obtained at 77 K (samples Nos. 2 and 4), the scope of the plateau became more pronounced at the lower temperature. For example, from the 77-K equipotential pattern for sample 4 [Figs. 12(c) and 12(d)], it can be deduced that the fraction of the total voltage drop over the sample represented by the plateau region has decreased at 77 K.

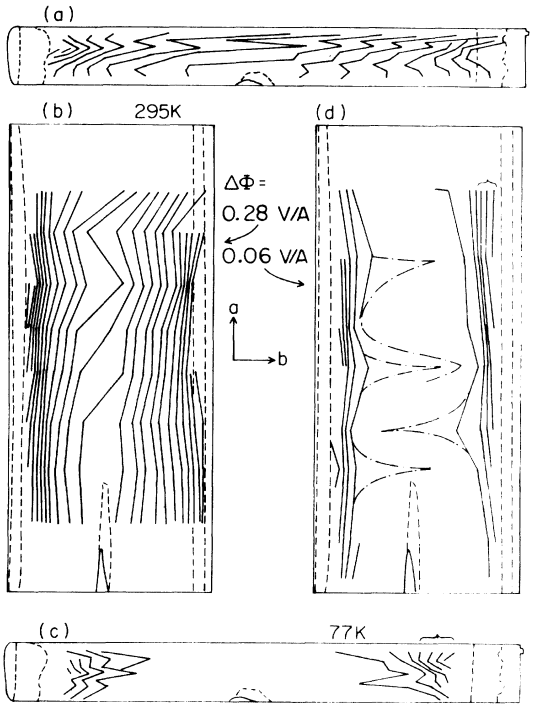

FIG. 12. Equipotential patterns for sample No. 4 obtained with EBCOM. Sample dimensions are 2.353 × 0.268 × 0.038 mm. (a) Room-temperature pattern; potential interval is 0.416 V/A. (b) Isotropic equivalent of (a) assuming $\sigma_b/\sigma_a = 400$. Potential interval is 0.278 V/A. (c) and (d) 77 K patterns; in region indicated by brackets, only every other equipotential line is plotted for clarity. Potential intervals are 0.056 V/A. Sample width in (d) is expanded 20 times with respect to length for visual convenience. Dot-dash curves indicated uncertainties in the equipotential curves.

In the regions where a plateau was observed, the plane of the sample surface was broken into a segment (two segments in the case of sample 4), extending the width of the sample, such that the plane defined by the segment was canted slightly with respect to the plane of the remaining surface. The orientation of the cant may be visualized by imagining each segment to be rotated slightly about an axis lying in the plane of the segment and parallel to the a axis. The surface imperfections are invisible in micrographs obtained with transmitted light, near-normal reflected light, and the SEM. Their presence can be revealed by observing the samples with reflected light microscopy but under conditons which enhance contrast between differently oriented planes. We emphasize that the segmented structure is quite common, being observable in over half the unmounted crystals examined, but also note that in mounted samples, not all segments produced plateaus.

Two possibilities for the origin of the plateaus are

possible. Regions of the sample with larger than average σ_b would produce plateaus, but such an explanation is unlikely in view of the fact that σ_b would have to be unrealistically large to account for the observed effect in all cases except one (in sample 1): calculating σ_b at the plateau by Eq. (12) gives room-temperature values of 2400 and 1100 $(\Omega\,\mathrm{cm})^{-1}$ for sample 2, 1300 $(\Omega\,\mathrm{cm})^{-1}$ for sample 3, and 945 and 563 $(\Omega\,\mathrm{cm})^{-1}$ for sample 1. A lower limit on σ_b of about 2500 $(\Omega\,\mathrm{cm})^{-1}$ is found for sample 4. Moreover, calculating the conductivity of sample 2 with the method of placing cross sections on either side of the plateau [Eq. (14)], applied to mechanical-probe data (where modulation broadening plays no role) gives *below* average values for σ_b, whereas an above average value should be calculated if the plateau represented a region of high σ_b.

It is more likely that those segments over which plateaus were observed are to some extent electrically isolated from the bulk of the sample. We have already noted the laminar structure of the samples and the sensitivity the potential distribution exhibits to separation of lamina when current is flowing primarily along the b axis. A physical separation explains qualitatively, but in a natural way, the details of the potential distribution in sample 4 [Figs. 12(a) and 12(b)]. If the segments were separated from the bulk and if the junctions between the segments and the adjacent surface lamina on either side were resistive, then the current density, and thus the electric field, in the segment would be reduced from that in the bulk. If, in addition, the junctions were inhomogeneously resistive, current would be expected to change course in the segment (as it does in Fig. 12) as it flowed between low-resistance points in each junction.

Attributing the plateaus to electrical discontinuities in the surface lamina is a plausible but speculative assertion in the absence of more complete experiments. Additional EBCOM experiments might include (i) improved-resolution scans (decreased modulation amplitude), in order to determine the behavior of the electric field on either side of the segments; (ii) measurements taken on both sides of the sample to search for correlations which would suggest a bulk origin to the plateau (the segments on the top and bottom surfaces appear uncorrelated); (iii) measurements taken with increased beam energies, and thereby increased penetration depths, which would allow one to probe the potential distribution within the bulk. For the 2.5-kV accelerating voltage used in our experiments it is expected, on the basis of the Bethe energy-range relation[25,44] and extrapolations of empirical data,[45–47] that less than 4% of the beam penetrates beyond 0.3 μm. Additional experiments could, of course, be undertaken with the mechanical probe. Potential plateaus are more easily discovered with EBCOM, however, because it is a derivative technique and as such is sensitive to changes in slope of the potential, and because it obtains data continuously over a scan. The mechanical-probe technique also suffers because the pressure of the probe, though slight, might press separated laminae together during the actual measurements.

E. Conductivity measurements

The methods derived in Sec. II C for computing the conductivity were applied to obtain, to a precision of approximately $\pm 15\%$, σ_b at room temperature for all ten samples, and σ_a (better than $\pm 5\%$) for the five point-contact samples; the results are summarized in Table I. Table II contains the results obtained at low temperatures.

Table I serves to establish the range of conductivities measured for our group of samples, to indicate the kind of precision obtainable, and to compare quantitatively the EBCOM and mechanical contact experiments. Since the potential plateaus found in samples 1 through 4 are a likely consequence of sample imperfections, σ_b for these samples was computed after omitting the data from the plateau region. The uncertainties for σ_b listed in Table I represent standard deviations about the mean of a number of computations carried out for different cross sections and for the most part reflect the noise-limited 10%–15% precision of the experiments. In the point-contact arrangements suitable for computing σ_a the electric field parallel to the a axis was nearly constant over most of the sample; consequently, σ_a was determined from the electric field in the center of the sample. The uncertainties given for σ_a indicate the *maximum* variation one would obtain if a representative electric field were chosen at some point other than the center, but still on a line bisecting the sample width.

An average of the b-axis conductivities, excluding sample 10, gives a σ_b of 490 $(\Omega\,\mathrm{cm})^{-1}$, somewhat higher than the mean conductivities reported by most groups. The spread in the conductivities ranges between 400 and 630 $(\Omega\,\mathrm{cm})^{-1}$, with seven of the nine samples falling between 400 and 500 $(\Omega\,\mathrm{cm})^{-1}$. Because the spread in σ_b of our sample set is greater than the uncertainty in our measurements, we believe that at room temperature there are real differences in σ_b from sample to sample. However, our spread is smaller (as was that of Bickford and Kanazawa) than that reported by most groups who use fixed contact techniques and it is important to state the possible factors which might account for the tighter range. The samples were carefully screened and so represent the most flawless crystals ($\sim 1\%$ from any given batch); nonetheless, the sample set itself (nine crystals) is smaller than many reported, so that rare crystals in the wings of the σ_b statistical distribution are less likely to have been measured.

TABLE II. Low-temperature conductivities. Room-temperature values are based on averages of mechanical probe and EBCOM data in those cases where data were taken with both techniques. Numbers in parentheses give the conductivity normalized to the room-temperature value. All values are in units of $(\Omega\,\mathrm{cm})^{-1}$.

Sample No.	Technique	a or b axis σ	T_r	77 K	60 K	45 K
2	EBCOM	b	~480	9600		
			(1)	(20)[a]		
4	EBCOM	b	~530	8600 ± 1000		
			(1)	(16)[a,b]		
9	PROBE	b	~430	5100 ± 1000		
			(1)	(12)		
		a	1.15	2.96 ± 0.18	2.81 ± 0.11[b]	0.69 ± 0.04
			(1)	(2.57)	(2.44)	(0.60)
10	EBCOM	a	1.11		3.01 ± 0.24	0.58 ± 0.03
			(1)		(2.71)	(0.52)

[a]Indicative only; see text. [b]62 K.

The spread in conductivities observed by groups relying on silver-paint voltage electrodes can be artifically broadened because of the finite extent of electrodes and because of inhomogeneous current paths. Thus, the spread *among* groups using different conventions for determining the distance between electrodes will be unavoidably broadened and as well, *within* a group, the inhomogeneous nature of the finite extend contact will introduce errors from sample to sample.[7]

We must refrain from drawing the conclusion that contact imperfections solely are contributing to the spread seen by most groups: our electrolytic tank experiments (carried out with voltage electrodes of zero extent along the b axis) indicate that contact inhomogeneities of moderate proportions will not much affect four-probe measurements of $\sigma_b(T_r)$ as long as the samples have a large l/w (greater than 10) and the electrodes are not too near one another.

V. SIMULATION EXPERIMENTS

A. Experimental

To determine the effect of contact inhomogeneities on conventional four-probe measurements of σ_b at low temperatures, we performed a series of experiments with imperfectly shaped electrodes in an electrolytic tank which represented the van der Pauw isotropic equivalent of an anisotropic sample. Three important results have come from our measurements: (a) assuming that the intrinsic peak σ_b is 21 times the room-temperature value, we have found spurious $\sigma_b(T)$ curves which mimic rather closely reported extraordinary crystals; (b) assuming that all samples are identical except for the contact inhomogeneities and sample dimensions we find that a statistical distribution of inhomogeneities leads to a statistical distribution of peak conductivities which resembles qualitatively the distribution reported by two groups[4,8]; (c) we have examined two tests by which spurious peak conductivities are said to be identifiable[10,14]; our evidence suggests that the so-called lead-switching test[14] is the more reliable.

Using the van der Pauw transformation of Eq. (1), it can be shown that the apparent b-axis conductivity measured with inhomogeneous contacts is in error by the same factor as the apparent electrolyte conductivity measured in the isotropic equivalent tank outfitted with correspondingly shape contacts

$$\sigma_b^m = (\sigma_t^m/\sigma_t)\sigma_b \ , \tag{17}$$

where σ_t and σ_b are, respectively, the intrinsic electrolyte and sample conductivities, and superscript m denotes values measured with the imperfect contacts.

To determine how a particular contact configuration affects the measured temperature dependence of σ_b, the dimensions of the tank must be altered in accordance with the temperature dependence of the conductivity anisotropy; from Eq. (1),[48] we have

$$l'/w' = (\sigma_a/\sigma_b)l/w \ . \tag{18}$$

Since d' changes only slightly with temperature, it was kept constant for convenience. $\sigma_b^m(T)$ curves are constructed with Eq. (17) after σ_t^m/σ_t is measured as a function of l'/w' and after three intrinsic properties are assigned to the hypothetical crystal which the tank is simulating: l/w, the temperature

dependence of the anisotropy $\sigma_b(T)/\sigma_a(T)$, and finally $\sigma_b(T)$. Our analysis was performed assuming the temperature dependence of the anisotropy to be that of Fig. 4(a) in Ref. 10 and $\sigma_b(T)$ to be the curve in Fig. 6 of the same reference with a peak normalized value of 21, redrawn in our Fig. 13.

The electrolytic tank, drawn schematically in Fig. 13, was constructed from Plexiglass with dimensions approximately $33 \times 40 \times 5$ cm and filled with tap water of conductivity near 3×10^{-4} $(\Omega\,\text{cm})^{-1}$. A movable plastic wall allowed the 33-cm length to be decreased to achieve smaller l'/w'. Current electrodes, fashioned from brass shim, were placed at either end of the tank, while the brass voltage electrodes were suspended from movable plastic rails located over the dotted lines in Fig. 13. An ac voltage of 1 kHz was applied to the current electrodes, and the voltage was measured with a digital voltmeter between the voltage electrodes. From the current, voltage, and spacing between voltage electrodes, σ_t^m was determined; this, together with the previously measured true conductivity, determined the error factor σ_t^m/σ_t for any particular electrode shape and l'/w'.

Out of the infinite number of possibilities for shaping inhomogeneous current and voltage electrodes, we chose the following. Each electrode was comprised of two separate pieces of brass, each piece being $\frac{1}{4}w'$ wide. The two pieces in each *current* electrode extended the entire depth of the tank and were arranged permanently as shown in the plan view of Fig. 13. The width of the tank was imagined as divided into four quarters, and the two pieces of each *voltage* electrode were allowed to slide along the plastic rail so that they could be suspended over any two of the imaginary quarters and lowered until they just broke the water surface. By measuring as a function of l'/w' the error factor associated with the 36 possible combinations (actually only 21 are unique) of the voltage electrode pieces, it is possible to obtain a statistical distribution of the possible erroneous conductivities which would be measured with inhomogeneous contacts on an otherwise perfect sample.

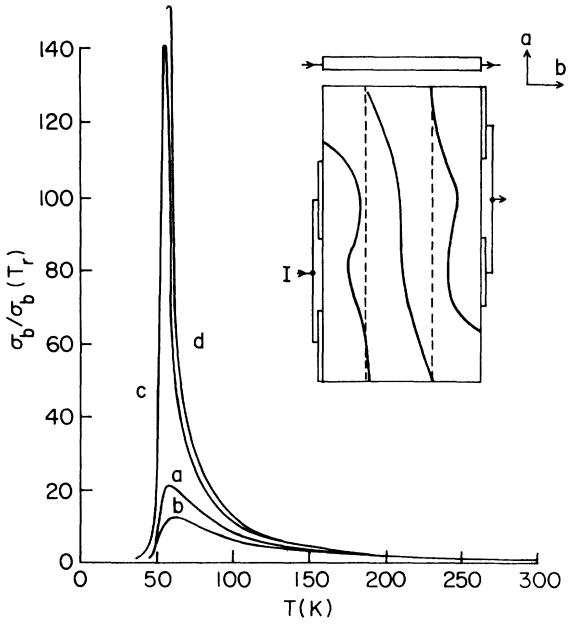

FIG. 13. *Apparent* normalized *b*-axis conductivity measured with inhomogeneous electrodes in the electrolytic tank: (a) conductivity from Ref. 2 which was assumed to be intrinsic for the data analysis; (b) underestimated and (c) overestimated peaks measured in the tank; (d) a large conductivity peak from Ref. 10 for temperatures above 58 K; the conductivity for lower temperatures is not shown for clarity. Inset: Schematic of electrolytic tank and its current electrodes. Voltage electrodes were placed over dotted lines; a particular set is shown. Equipotentials (in absence of voltage electrodes) are also indicated.

Contact resistance was simulated by placing a discrete resistor between each piece of a given voltage electrode and the voltmeter. The resistors prevented the two pieces of the electrode from shorting out potential differences which exist across the transverse dimensions of the tank as a consequence of the contact inhomogeneities [see discussion following Eq. (16)]. The size of the resistors was selected so that their parallel combination was commensurate with the contact resistances of Ref. 10 appropriately scaled to the electrolytic tank's resistance. The inclusion of the contact resistance generally had a small effect ($\pm 20\%$ in the error factor), but for those contact configurations which produced enhancements in the error factor at small l'/w', the inclusion of the contact resistance caused the error factor to increase by as much as a factor of 2.

B. Results

The temperature dependence of σ_b^m for a few selected contact configurations is shown in Fig. 13, along with two curves taken from Fig. 6 of Ref. 10, one exhibiting a large and the second a common peak conductivity. The σ_b^m curves demonstrate that, unlike those curves of apparent conductivity generated both experimentally[14] and theoretically[13] with four contacts, the temperature dependence of $\sigma_b^m(T)$ obtained from our more realistic tank electrodes closely resemble published data for both above- and below-average peaks.

The error factor σ_t^m/σ_t exhibited functional dependences on l'/w' which have important consequences for both the $\sigma_b^m(T)$ curves and the statistical distribution of peak conductivities discussed below. For contact configurations which caused substantial error, the error factor rose or fell *monotonically* with decreasing l'/w', with the dependence on l'/w' becoming stronger at smaller l'/w'. Because of the monotonic

dependence, the temperature of the peak in σ_b^m is altered slightly but systematically. For example, the $\sigma_b^m(T)$ curves in Fig. 13 peaked at 56 K for the enhanced and at 61 K for the depressed, while the assumed intrinsic conductivity peaked at 58 K. Unfortunately, because in our model the temperature T_p at the peak depends sensitively on the assumed $\sigma_b(T)$ and $\sigma_b(T)/\sigma_a(T)$, and because differences in the intrinsic properties are expected, the shift of T_p (downward for enhanced conductivities) cannot be regarded as diagnostic of contact problems; the size of the spread in T_p, however, is consistent with reported variations[8,10] between 56 and 65 K.

Three hypothetical crystals with l/w of 24, 18, and 12, each "mounted" 36 times with the contact configurations detailed previously, generated the statistical distribution of peak conductivities appearing in Fig. 14(c). For the 12:1 sample, one of the 36 contact configurations produced an infinite σ_b which subsequently went negative near 58 K; this datum has been discarded. The statistics obtained from two research groups[4,8] are displayed in Figs. 14(a) and 14(b). In order to maintain a constant bin size, the bars marked with dots in Fig. 14(a) were assigned arbitrary positions consistent with the ranges given in Ref. 4. The authors of the paper[8] from which Fig. 14(b) was constructed have determined, on the basis

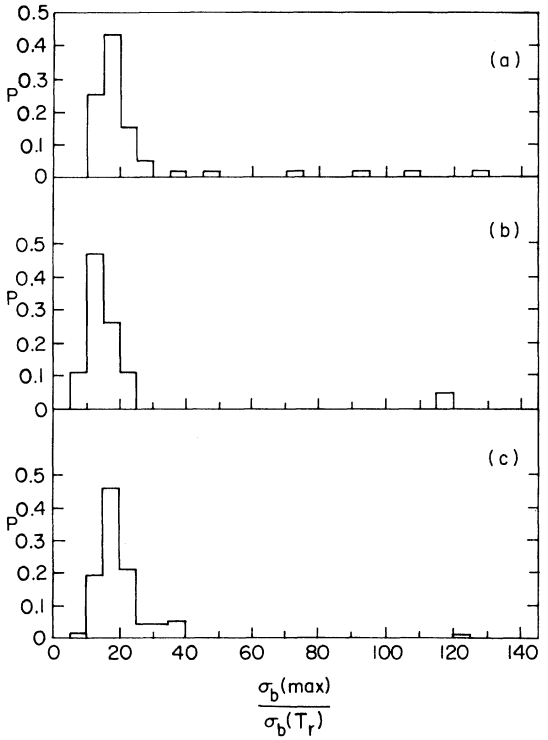

FIG. 14. Histograms of statistical distribution of peak σ_b^m normalized to room temperature from: (a) Ref. 4; (b) Ref. 8; (c) electrolytic tank. P is probability per bin.

of lead switching tests, that the isolated peak at 120 is a consequence of inhomogeneous current paths.

A number of similarities among the three sets of statistics bear mentioning: all three distributions exhibit a significant spread near a peak normalized conductivity of 20. All three probability distributions exhibit an extended tail on the high-peak side which quickly becomes very small for large peak conductivities.

The similarity between the probability distributions obtained with the simulation experiments and with real samples suggest that inhomogeneous current paths could be playing an important role, perhaps as important as intrinsic sample differences, in the distribution of peak conductivities measured by many groups: more-concrete conclusions would be premature at this point, especially in light of the probabilistic basis of any conjecture, and because of the experimental qualifications which we briefly reiterate. The inhomogeneous contacts used in the electrolyte tank are less homogeneous than usually found (evidenced by the negative conductivity mentioned above) and have zero extent along the sample length. Further, variations in the intrinsic properties $\sigma_b(T)/\sigma_a(T)$, have not been folded into our analysis. Finally, sample imperfections have not been included in the simulation experiments. Imperfections are expected to play a role because, first, cracks have been demonstrated in our movable sensor data to be important in some cases, and second, because temperature cycling has been shown to cause spurious enhanced peaks and eventually to reduce significantly the peak conductivity.[8,10]

The above qualifications do not substantially affect a number of important results. Most importantly, unusually large or small peaks in $\sigma_b(T)$ curves resembling those reported may be a consequence of inhomogeneous current paths. In addition, for a given sample, the smaller l'/w' is for the isotropic equivalent at T_p, the more extreme will be the overestimate or underestimate of the peak-normalized conductivity $\sigma_b^m(T_p)/\sigma_b^m(T_r)$. This is so because σ_b^m/σ_b varies more and more rapidly as l'/w' becomes smaller. Thus, from Eq. (18), samples with small l/w (less than 10 is small for TTF-TCNQ) *or* large $\sigma_b(T_p)/\sigma_a(T_p)$ will exhibit the largest extremes in normalized conductivity. Because the anisotropy near T_p is dominated by the magnitude of σ_b, as shown from Montgomery four-probe measurements.[10] *high quality groups of crystals with superior* σ_b *have the greatest chance of producing spuriously large* $\sigma_b^m(T_p)$. Finally, the distance separating the voltage electrodes, relative to the sample length, is profitably kept large in order to avoid spurious large peaks: a larger separation reduces the chance that lines of constant potential will run (or nearly run) beneath *both* voltage electrodes. Under such conditions, the probability of *significantly* overestimating or underestimat-

ing $\sigma_b(T)$ is increased. (This reasoning is borne out in the tank for the contact configuration which gave the largest enhancement: for a 20:1 sample at 60 K, the error factor from electrodes separated by $\frac{1}{2}l$ was 1.7 vs 3.2 for electrodes separated by $\frac{1}{3}l$.)

C. Tests for inhomogeneous current paths

Two tests have been proposed[10,14] as a means of identifying whether or not inhomogeneous currents are affecting σ_b^m. In the first test,[10] $\sigma_b^m(T)$ is examined near 40 K for the existence of a second peak. In the second,[14] the functions of two leads, a current and a voltage lead, are interchanged and the voltage is remeasured; if the second voltage is a substantial fraction of the original, inhomogeneous currents are implicated. Evidently, there has been some confusion regarding the validity of the tests[49]; consequently, we briefly examined each test in the tank. We find that both tests are based on sound reasoning (in fact, both tests have been used successfully)[9,10] but that the lead switching test is generally the more sensitive and conclusive.

The double-peak test was first proposed by Cohen *et al.*[10] after they discovered, by using the Montgomery point-contact method, that σ_b/σ_a exhibited a peak at 40 K, as well as (for the better samples) at 55 ± 3 K. The possible existence of a second peak in $\sigma_b^m(T)$ imposed by inhomogeneous currents is predicted by Eq. (18): l'/w' will exhibit an extremum whenever the anisotropy, σ_b/σ_a, does. Because the measured error factor σ_t^m/σ_t is generally a monotonic function of l'/w', it too possesses an extremum in magnitude whenever the anistropy does. The sensitivity of the test, however, depends not on σ_t^m/σ_t, but on the possibility of a second peak appearing at 40 K in σ_b^m; that is, in the *product* $(\sigma_t^m/\sigma_t)\sigma_b$. As pointed out by other authors,[49] the effect on σ_b^m of extrema in the error factor is greatly reduced when the intrinsic σ_b is relatively small; moreover, when $\sigma_b(T)$ is falling rapidly with temperature (as it is near 40 K), the second peak in σ_b^m can be completely suppressed, although some remnant of the extremum in the error factor will always persist in σ_b^m. Because it has been found that the intrinsic $\sigma_b(T)$ undergoes a distinct drop at 38 K,[11,22,50] the existence of the small remnant is likely to be unclear (as has been argued by Etemad).[11]

Our tank experiments show that the magnitude of the effect of the peak in anisotropy at 40 K on σ_b^m when inhomogeneous currents are present depends crucially on the magnitude of the intrinsic σ_b. For example, using a contact configuration which enhanced $\sigma_b^m(T)$, and analyzing the tank results for $\sigma_b^m(T)$ as before, but this time with the intrinsic $\sigma_b(T)$ assumed to resemble that of Etemad[11] in the temperature range 38 to 44 K (with the drop at 38 K smoothed over), we found that $\sigma_b^m(T)$ exhibited only a slight perturbation at 38 to 40 K although it had reached a spurious peak at 58 K, 3.5 times the true peak value; for a sample aspect ratio chosen to give a spurious peak at 58 K of 6.7 times the intrinsic value, there did appear a small local maximum in σ_b^m (40 K), although the small size of the maximum would very likely go unnoted in a linear plot of $\sigma_b^m(T)$ of sufficient scale to include the peak.

The second test for inhomogeneous currents, proposed by Schaefer *et al.*,[14] compares the voltage V_c measured when a current and voltage lead are interchanged (or "crossed"), to the voltage V measured with the usual four-probe arrangement; in the crossed configuration, current flowing inhomogeneously between two adjacent electrodes at one end of the sample are expected to produce a voltage drop between the remaining two electrodes. Although even perfect contacts will effect a voltage drop in the crossed configuration (as first pointed out by Cohen *et al.*[10]), our tank experiments show that V_c in the presence of inhomogeneous currents is significantly larger than V_c for perfect contacts.

Perfect contacts were simulated in the tank, and the voltage ratio V_c/V was measured as a function of the tank aspect ratio l'/w'. V_c/V increased from 2.1×10^{-4} for l'/w' of 0.48 to 5.1×10^{-3} for l'/w' of 0.12. For the contact configuration which produced the largest enhancements, the behavior of V_c/V as a function of temperature resembled that found on a real sample by Gemmer *et al.*[9]; V_c/V rose from 0.09 (error factor 1.26) to 3.2 (error factor 5.6). A spot check of other electrode configurations for l'/w' of 0.24 showed that in general, even modest enhancements were accompanied by V_c/V of 0.6 or more. In one trial, both the current and voltage electrodes were positioned in an effort to evade the test. In the closest evasion, an error factor of 4.8 was associated with V_c/V of 0.045, still an order of magnitude greater than perfect contact V_c/V. Of course we cannot unequivocally state that the test is perfect; unlike the case of the two-peak test, however, considerable effort would be required to contrive a contact configuration which would enhance σ_b^m and still circumvent the lead switching test at all temperatures. Finally, we note that the lead switching tests also indicates when σ_b^m is *underestimated* as a consequence of inhomogeneous currents (although in some cases with less sensitivity), and can be used on materials *without* double peak signatures.

VI. SUMMARY

We have demonstrated that an electron beam can be used to determine the potential distribution that would be produced by current flowing in small samples of modest conductivity [1 to 10^4 $(\Omega\,\mathrm{cm})^{-1}$].

The results are of sufficient precision that sample conductivities may be obtained from the potential distribution by using formulas derived in Sec. II C. The flexibility of the technique promises as yet untried possibilities in the range of problems which may be attacked. It should be possible, for example, to extend the accessible conductivities to beyond 10^5 $(\Omega\,\mathrm{cm})^{-1}$ with a resolution of better than 1 μm for certain contact configurations if specimen currents of 1 μA can be used and if specimens are thin enough (< 50 μm).

We applied the technique to the organic, highly anisotropic metal, TTF-TCNQ. The movable beam results were confirmed and complemented with the conventional movable pressure contact method of determining potential distributions. Samples with pointlike contacts and with extended contacts were examined. In nearly all cases, evidence for contact inhomogeneity was found, but the effects of the inhomogeneities on the expected potential distribution were small for the point-contact configurations. Some samples appearing above average in morphology were found to exhibit irregularities in the potential distribution correlated to sample imperfections observed in detailed optical and scanning electron micrographs. In particular, potential irregularities consistent with hypothesized separation of sample lamina were found to be widespread and were correlated to the occurrence of a previously unreported segmented surface structure. The nature of the potential distribution associated with this surface structure is such that both over and underestimates of conductivity are possible with four-probe measurements.

Despite irregularities in the potential distribution, our methods of analysis allowed a determination of the b-axis conductivity; we obtained an average value of 490 ± 80 $(\Omega\,\mathrm{cm})^{-1}$, comparable to but somewhat greater than the average values reported by other groups.

Both the movable beam technique and the movable contact technique were extended to low temperature with partial success. Difficulties in each technique were discussed and possible solutions suggested. The results showed that sample flaws in TTF-TCNQ were more disruptive at low temperature (above the metal-insulator transition) than at room temperature. The conductivities determined at 77 K were consistent with average conductivities reported in the literature.

The quantitative errors which contact inhomogeneities effect in conventional four-probe measurements were studied in an electrolytic tank. The results showed that there exists a small probability of measuring conductivities with enhanced peaks, the temperature dependence of which resembles published data. The appearance at low temperatures of a second peak in the measured b-axis conductivity as a test of spurious peaks was found to be less adequate in some cases than a lead switching test.

ACKNOWLEDGMENTS

We wish to thank John Arao for his assistance in making measurements in the electrolytic tank. We also thank Dr. G. DePasquali who grew the samples we used. This work was supported in part by the U.S. Department of Energy under Contract No. EY-76-C-02-1198.

---

*Now at Cornell University, Ithaca, N.Y.

[1]H. R. Zeller, Adv. Solid State Phys. 13, 31 (1973).
[2]I. F. Shchegolev, Phys. Status Solidi A 12, 9 (1972).
[3]G. A. Thomas, D. E. Schafer, F. Wudl, P. M. Horn, D. Rimai, J. W. Cook, D. A. Glocker, M. J. Skove, C. W. Chu, R. P. Groff, J. L. Gillson, R. C. Wheland, L. R. Melby, M. B. Salamon, R. A. Craven, G. DePasquali, A. N. Bloch, D. O. Cowan, V. V. Walatka, R. E. Pyle, R. Gemmer, T. O. Poehler, G. R. Johnson, M. G. Miles, J. D. Wilson, J. P. Ferraris, T. F. Finnegan, R. J. Warmack, V. F. Raaen, and D. Jerome, Phys. Rev. B 13, 5105 (1976).
[4]M. J. Cohen, L. B. Coleman, A. F. Garito, and A. J. Heeger, Phys. Rev. B 13, 5111 (1976).
[5]L. B. Coleman, M. J. Cohen, D. J. Sandman, F. G. Yamagishi, A. F. Garito, and A. J. Heeger, Solid State Commun. 12, 1125 (1973).
[6]L. R. Bickford and K. K. Kanazawa, J. Phys. Chem. Solids 37, 839 (1976).
[7]R. P. Groff, A. Suna, and R. E. Merrifield, Phys. Rev. Lett. 33, 418 (1974).
[8]R. V. Gemmer, D. O. Cowan, T. O. Poehler, A. N. Bloch, R. E. Pyle, and R. H. Banks, J. Org. Chem. 40, 3544 (1975).
[9]R. V. Gemmer, D. O. Cowan, A. N. Bloch, R. E. Pyle, and R. H. Banks, Mol. Cryst. Liq. Cryst. 32, 237 (1976).
[10]M. J. Cohen, L. B. Coleman, A. F. Garito, and A. J. Heeger, Phys. Rev. B 10, 1298 (1974).
[11]S. Etemad, Phys. Rev. B 13, 2254 (1976).
[12]J. P. Ferraris and T. F. Finnegan, Solid State Commun. 18, 1169 (1976).
[13]R. J. Warmack, T. A. Callcott, and H. C. Schweinler, Appl. Phys. Lett. 24, 635 (1974).
[14]D. E. Schafer, F. Wudl, G. A. Thomas, J. P. Ferraris, and D. O. Cowan, Solid State Commun. 14, 347 (1974).
[15]T. E. Phillips, T. J. Kistenmacher, J. P. Ferraris, and D. O. Cowan, Chem. Commun. 471 (1973).
[16]G. T. Meaden, *Electrical Resistance of Metals* (Plenum, New York, 1965).
[17]J. Ferraris, D. O. Cowan, V. Walatka, Jr., and J. H. Perlstein, J. Am. Chem. Soc. 95, 948 (1973).
[18]S. Etemad, T. Penney, E. M. Engler, B. A. Scott, and P. E.

Seiden, Phys. Rev. Lett. 34, 741 (1975).
[19]S. K. Khanna, E. Ehrenfreund, A. F. Garito, and A. J. Heeger, Phys. Rev. B 10, 2205 (1974).
[20]A. N. Bloch, J. P. Ferraris, D. O. Cowan, and T. O. Poehler, Solid State Commun. 13, 753 (1973).
[21]M. Cohen, S. K. Khanna, W. J. Gunning, A. F. Garito, and A. J. Heeger, Solid State Commun. 17, 367 (1975).
[22]W. N. Hardy, A. J. Berlinsky, and L. Weiler, Phys. Rev. B 14, 3356 (1976).
[23]H. C. Montgomery, J. Appl. Phys. 42, 2971 (1971).
[24]D. Zosel, H. Ritschel, and H. Hansel, Phys. Status Solidi 38, 183 (1970).
[25]J. P. Long, Ph.D. thesis (University of Illinois, 1977) (unpublished).
[26]G. D. Monteath, *Applications of the Electromagnetic Reciprocity Principle* (Pergamon, New York, 1973).
[27]L. J. van der Pauw, Philips Res. Rep. 16, 187 (1961).
[28]P. R. Thornton, *Scanning Electron Microscopy* (Chapman and Hall, London, 1968).
[29]T. E. Everhart, and T. L. Hayes, Sci. Am. 226, 54 (1972).
[30]C. Munakata, Jpn. J. Appl. Phys. 5, 756 (1966).
[31]P. M. Chaikin, J. F. Kwak, T. E. Jones, A. F. Garito, and A. J. Heeger, Phys. Rev. Lett. 31, 601 (1973).
[32]J. F. Kwak, P. M. Chaikin, A. A. Russel, A. F. Garito, and A. J. Heeger, Solid State Commun. 16, 729 (1975).
[33]J. F. Nye, *Physical Properties of Crystals* (Oxford U.P., London, 1957).
[34]A. R. Billings, *Tensor Properties of Materials* (Wiley-Interscience, London, 1969).
[35]J. D. Wasscher, Philips Res. Rep. 16, 301 (1961).
[36]J. Hornstra and L. J. van der Pauw, J. Electron. Control 7, 169 (1959).
[37]S. V. Airapetyants and M. S. Bresler, Sov. Phys. Solid State 1, 134 (1959).
[38]J. Juretschke, *Crystal Physics* (Benjamin, Reading, Mass., 1974).
[39]C. W. Oatley, *The Scanning Electron Microscope* (Cambridge U.P., Cambridge, England, 1972).
[40]C. D. Motchenbacher and F. C. Fitchen, *Low Noise Electronic Design* (Wiley, New York, 1973).
[41]A modulation frequency of 10 kHz was chosen to avoid thermoelectric signals which were substantial below 2 kHz.
[42]M. Walter and L. Ramaley, Anal. Chem. 45, 1965 (1973).
[43]See note 22 in Ref. 3.
[44]C. R. Worthington and S. G. Tomlin, Proc. Phys. Soc. London Ser. A 69, 401 (1956).
[45]V. E. Cosslett and R. N. Thomas, Br. J. Appl. Phys. 15, 883 (1964).
[46]V. E. Cosslett and R. N. Thomas, Br. J. Appl. Phys. 15, 1283 (1964).
[47]V. E. Cosslett and R. N. Thomas, Br. J. Appl. Phys. 16, 779 (1964).
[48]By altering the tank dimensions in such a manner, we have implicitly assumed the principal axes of the conductivity tensor to be coincident with the *a*, *b*, and c^* axes. An exact treatment would require knowing the principal axes and would skew the tank cross section. Because samples are thin, a large degree of skew is necessary to affect our results; such a skew is lacking, at least at room temperature, because it could have otherwise been observed in the equipotential patterns of our point-contact samples.
[49]See note 9 in Ref. 3 and note 35 in Ref. 4.
[50]C. W. Chu, J.M.E. Harper, T. H. Geballe, and R. L. Greene, Phys. Rev. Lett. 31, 1491 (1973).